J. Sound Vib. (1969) **9** (3), 469–486

SOUND TRANSMISSION USING STATISTICAL ENERGY ANALYSIS

M. J. CROCKER AND A. J. PRICE

Department of Building Science, University of Liverpool, Liverpool 3, *England*

(*Received* 31 *July* 1968)

Statistical energy analysis is used to predict the sound transmission loss, the radiation resistance and the vibration amplitude of a partition. Agreement between theory and experiment is shown to be good. The "mass-law" sound transmission is seen to be due to non-resonant modal vibration while the increased transmission in the coincidence region is seen to be due to resonant modal vibration. The observed vibration amplitude is also shown to be due to resonant modes. The previously observed discrepancy between the values of vibration amplitude derived from the mass law and those observed experimentally which has been described in the literature [1] is thus satisfactorily explained.

1. INTRODUCTION

In recent years new techniques have been developed for predicting the acoustic response and radiation properties of complicated structures [2–6]. These techniques sometimes known as "statistical energy methods" have been primarily applied to predicting the noise and vibration levels in aircraft and spacecraft structures. In the past, the classical architectural sound transmission problem has normally been approached theoretically with so-called "mass-law theories" [7–11]. Often these theories neglect damping and stiffness in the partition, which is assumed to be infinite in extent and to respond as a limp membrane. In this paper the classical sound transmission problem is approached using statistical energy methods. This approach includes panel stiffness and damping and the effects of finite panel size and successfully predicts the panel vibration amplitude and the dip in the transmission loss curve at the coincidence frequency.

Theory developed by Lyon [12, 13] and Ungar [14] is used to predict the partition transmission loss and vibration amplitude in section 5 of the paper. The present authors have extended this theory in sections 4.2 and 4.4 of the paper to enable the partition radiation resistance and its coupling with the transmission rooms to be determined. In order to predict the partition transmission loss and vibration amplitude it is necessary to know the radiation resistance of the partition. Both theoretical values (due to Maidanik [4]) and experimental values (determined using the analysis developed in section 4.2) were used in the predictions.

Utley and Mulholland [1] have recently shown that the vibration amplitude of a partition is very much greater than that predicted by mass law. This discrepancy is easily explained by the present approach. As is shown in this paper, the vibration amplitude at any frequency is due to the response of resonant modes. The vibration amplitude is thus governed by the total resistance and by the radiation resistance of the panel at any particular frequency. It is found that using a measured value of the partition total resistance, it is possible to predict the vibration amplitude to within 1 or 2 dB throughout the frequency range 400 to 10,000 Hz.

2. MODAL BEHAVIOUR OF PANEL

The resonant modes of a panel can be divided into two classes. Modes with resonance frequencies above the critical or coincidence frequency and thus having bending velocities

greater than the speed of sound in air are termed acoustically fast (A.F.). Modes with resonance frequencies below the critical frequency and thus having bending velocities less than the speed of sound are termed acoustically slow (A.S.).

It can be shown theoretically [4, 6] that the A.F. modes have a high radiation efficiency, whilst the A.S. modes have a low radiation efficiency. The A.S. modes may be further subdivided into two groups. A.S. modes which have bending phase speeds in one edge direction greater than the speed of sound and bending phase speeds in the other edge direction less than the speed of sound are termed "edge" or "strip" modes. A.S. modes which have bending phase speeds in both edge directions less than the speed of sound are termed "corner" or "piston" modes. Corner modes have lower radiation efficiencies than edge modes.

The theoretical results for the radiation efficiency and classification of modes can also be given a simple physical explanation. Figure 1 shows a typical modal pattern in a simply-supported panel. The dotted lines represent panel nodes.

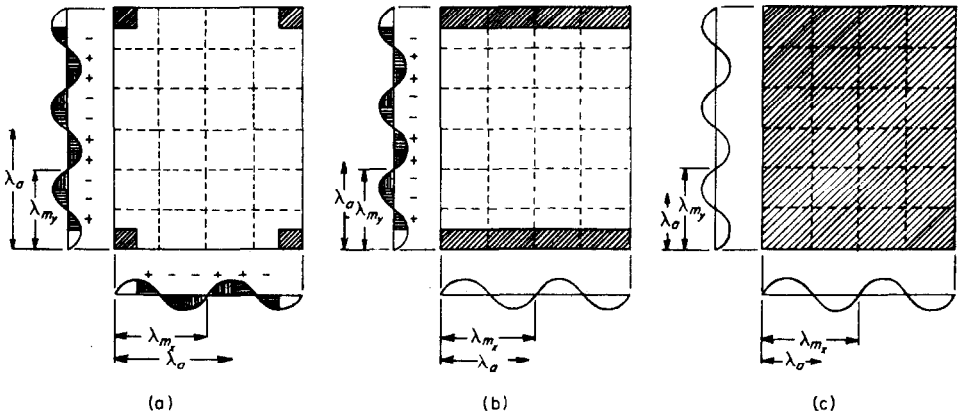

Figure 1. Wavelength relations and effective radiating areas for corner, edge and surface modes. (a) Corner mode; (b) X-edge mode; (c) surface mode. ■, Effective radiating area.

The modal vibration of a finite panel consists of standing waves. Each standing wave may be considered to consist of two pairs of bending waves, the waves of each pair travelling in opposite directions. Consider a mode which has bending wave phase speeds which are subsonic in directions parallel to both of its pairs of edges. In this case the fluid will produce pressure waves which will travel faster than the panel bending waves and the acoustic pressures created by the quarter wave cells [as shown in Figure 1(a)] will be cancelled everywhere except at the corners as shown. If a mode has a bending wave phase speed which is subsonic in a direction parallel to one pair of edges and supersonic in a direction parallel to the other pair, then cancellation can only occur in one edge direction and for the mode shown in Figure 1(b), the quarter wave cells shown will cancel everywhere except at the x edges. Acoustically fast modes have bending waves which are supersonic in directions parallel to both pairs of edges. Then the fluid cannot produce pressure waves which will move fast enough to cause any cancellation and the result is shown in Figure 1(c).

Since A.F. modes radiate from the whole surface area of a panel, they are sometimes known as "surface" modes. With surface modes the panel bending wavelength will always match the acoustic wavelength traced on to the panel surface by acoustic waves at some particular angle of incidence to the panel; consequently, surface modes have high radiation efficiency. This phenomenon does not happen for A.S. modes, the acoustic trace wavelength always being greater than the bending wavelength; A.S. modes have a low radiation efficiency.

At the critical frequency (when the panel bending wavelength equals the trace wavelength of grazing acoustic waves), the panel vibration amplitude is high (Figure 17). The radiation efficiency which is proportional to the radiation resistance is also high (Figure 12). Thus at the critical frequency the sound transmission is high and is due to modes resonant in a band centred at this frequency. Since the modes are resonant the transmission can be reduced effectively in this region by increasing the internal damping of the panel.

Well below coincidence the vibration amplitude of resonant modes is low and the radiation efficiency is also low. In this region it is usually found that more sound is transmitted by modes which are not resonant in the frequency band under consideration. Since these modes are not excited at their resonance frequencies they are little affected by internal damping. The contribution due to the non-resonant modes gives rise to the well-known "mass law" transmission. Just above coincidence the panel vibration amplitude and the radiation efficiency are high and the transmission is still resonant. However, as the frequency is increased further, the internal damping increases rapidly, the non-resonant transmission becomes more important, and the transmission again approaches mass law [15].

The relative importance of resonant and non-resonant transmission of course depends upon the practical structure under consideration and upon the variation of internal and radiation resistance with frequency. The radiation resistance is normally increased with the addition of stiffeners which will usually increase resonant transmission. An increase of internal damping which may be achieved in several ways including the use of rivetted structures or damping material will decrease resonant transmission and increase the importance of "mass law" transmission.

3. POWER FLOW BETWEEN COUPLED SYSTEMS

The power flow between coupled oscillator systems has been studied by several authors [3, 12, 16–18]. It is assumed that the power flow from one system to another is proportional to the difference in modal energies of the systems [3].

3.1. TWO COUPLED SYSTEMS

Consider the panel suspended in a reverberant room. The room may be considered as system 1 and the panel as system 2 as shown schematically in Figure 2. Following Lyon and

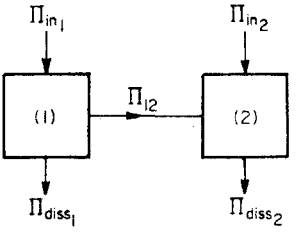

Figure 2. Block diagram representing energy flows between panel and reverberant room.

Scharton [12] the power flow balance for the two systems may be written [equations (1) to (4)]

$$\Pi_{in_1} = \Pi_{diss_1} + \Pi_{12}, \tag{1}$$

$$\Pi_{in_1} = \omega\eta_1 E_1 + \omega\eta_{12} n_1 \left(\frac{E_1}{n_1} - \frac{E_2}{n_2}\right), \tag{2}$$

$$\Pi_{in_2} = \Pi_{diss_2} - \Pi_{12}, \tag{3}$$

$$\Pi_{in_2} = \omega\eta_2 E_2 - \omega\eta_{12} n_1 \left(\frac{E_1}{n_1} - \frac{E_2}{n_2}\right), \tag{4}$$

where Π_{in_1} and Π_{in_2} are the rates of energy flow (in a frequency bandwidth of 1 rad/sec, centred on ω) into systems 1 and 2, respectively, supplied by a loudspeaker or shaker; Π_{diss_1} and Π_{diss_2} are the rates of internal dissipation of energy in systems 1 and 2 (in a bandwidth of 1 rad/sec); E_1 and E_2 are the total energies of systems 1 and 2 (in a bandwidth of 1 rad/sec). It should be noted that the coupling loss factor η_{12} strictly is only defined for zero energy in the second system [19], $E_2/n_2 = 0$, otherwise equations (2) and (4) do not balance. However, in most practical situations $E_2/n_2 \ll E_1/n_1$ and $\eta_{12} \approx \eta_{12}|_{E_2=0}$.

3.2. THREE COUPLED SYSTEMS

Consider the transmission suite shown in Figure 3. This may be considered to consist of three coupled systems as shown schematically in Figure 4. In a similar manner the power flow balance for the three systems may be written

$$\Pi_{in_1} = \Pi_{diss_1} + \Pi_{12} + \Pi_{13}, \tag{5}$$

$$\Pi_{in_1} = \omega\eta_1 E_1 + \omega\eta_{12} n_1 \left(\frac{E_1}{n_1} - \frac{E_2}{n_2}\right) + \omega\eta_{13} n_1 \left(\frac{E_1}{n_1} - \frac{E_3}{n_3}\right); \tag{6}$$

$$\Pi_{in_2} = \Pi_{diss_2} - \Pi_{12} + \Pi_{23}, \tag{7}$$

$$\Pi_{in_2} = \omega\eta_2 E_2 - \omega\eta_{12} n_1 \left(\frac{E_1}{n_1} - \frac{E_2}{n_2}\right) + \omega\eta_{23} n_2 \left(\frac{E_2}{n_2} - \frac{E_3}{n_3}\right); \tag{8}$$

$$\Pi_{in_3} = \Pi_{diss_3} - \Pi_{13} - \Pi_{23}, \tag{9}$$

$$\Pi_{in_3} = \omega\eta_3 E_3 - \omega\eta_{13} n_1 \left(\frac{E_1}{n_1} - \frac{E_3}{n_3}\right) - \omega\eta_{23} n_2 \left(\frac{E_2}{n_2} - \frac{E_3}{n_3}\right). \tag{10}$$

The Π_{13} term represents power flow from system 1 to system 3 when there are no modes excited in system 2 in the frequency band under consideration. Thus the power flow Π_{13} must

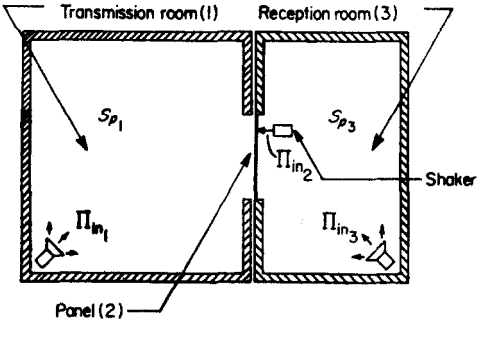

Figure 3. The transmission suite.

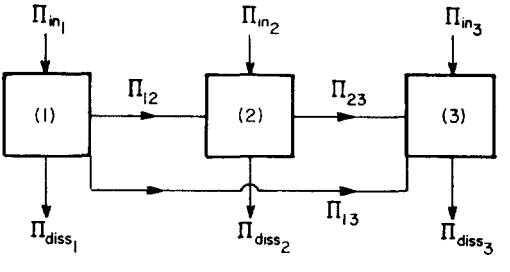

Figure 4. Block diagram representing energy flows between coupled systems of transmission suite.

be due to modes which are resonant outside of the frequency band under consideration. In this situation system 2 is non-resonant and acts only as a coupling element between systems 1 and 3. Providing the coupling factor is defined (i.e. a limp mass giving "mass law" power flow) this non-resonant power flow can be calculated. Since "mass law" transmission is derived assuming zero stiffness and damping in the partition and off resonance, these parameters are unimportant to the response; then Π_{13} can be derived from "mass law" transmission [13, 20].

4. PANEL RADIATION RESISTANCE AND COUPLING WITH ROOMS

4.1. RADIATION RESISTANCE OF PANEL IN REVERBERANT ROOM

Suppose a panel is suspended in a reverberant room and is excited by a shaker. The power flow is given by equations (1) to (4) with $\Pi_{\text{in}_1} = 0$. Making this substitution, equations (1) and (3) become equations (11) and (12), respectively:

$$0 = \Pi_{\text{diss}_1} + \Pi_{12}, \tag{11}$$

$$\Pi_{\text{in}_2} = \Pi_{\text{diss}_2} - \Pi_{12}. \tag{12}$$

Thus, combining equations (11) and (12),

$$\Pi_{\text{in}_2} = \Pi_{\text{diss}_2} + \Pi_{\text{diss}_1}. \tag{13}$$

The total power supplied to the panel by the shaker is

$$\Pi_{\text{in}_2} = E_2(R_{\text{tot}}/M_p) = M_p S_v(R_{\text{tot}}/M_p) = (S_a/\omega^2) R_{\text{tot}},$$

where

$$R_{\text{tot}} = R_{\text{int}} + R_{\text{rad}}.$$

The rate of energy dissipation by the panel in internal friction is

$$\Pi_{\text{diss}_2} = E_2(R_{\text{int}}/M_p) = (S_a/\omega^2) R_{\text{int}},$$

and the rate of internal energy dissipation by the room is

$$\Pi_{\text{diss}_1} = E_1 \beta_1 = [V_1 S_{p_1}/(\rho c^2)] \beta_1.$$

Substituting these expressions in equations (13) gives

$$(S_a/\omega^2) R_{\text{tot}} = (S_a/\omega^2) R_{\text{int}} + [V_1 S_{p_1}/(\rho c^2)] \beta_1,$$

and, on rearranging,

$$R_{\text{rad}} = \frac{\omega^2}{S_a \rho c^2} [S_{p_1} V_1 \beta_1]. \tag{14}$$

Equation (14) was used in the measurement of the radiation resistance described in section 6.3.1. of this paper. But $n_1 = (\omega^2 V_1)/(2\pi^2 c^3)$, thus equation (14) may be rewritten

$$R_{\text{rad}} = \frac{2\pi^2 c}{S_a \rho} [S_{p_1} n_1 \beta_1]. \tag{15}$$

Equation (15) is the result obtained by Lyon and Maidanik [3].

4.2. RADIATION RESISTANCE OF PANEL BETWEEN ROOMS

Suppose a panel is clamped between two reverberant rooms (Figure 3) and is excited by a shaker. The power flow is given by equations (5) to (10) with $\Pi_{\text{in}_1} = 0$ and $\Pi_{\text{in}_3} = 0$. Thus, with this substitution, equations (5) and (9) become equations (16) and (17), respectively:

$$0 = \Pi_{\text{diss}_1} + \Pi_{12} + \Pi_{13}, \tag{16}$$

$$0 = \Pi_{\text{diss}_3} - \Pi_{13} - \Pi_{23}. \tag{17}$$

Combining equations (16) and (17) and noting that since power flow must be directional, $\Pi_{21} = -\Pi_{12}$, gives equation (18):

$$\Pi_{\text{diss}_1} + \Pi_{\text{diss}_2} = \Pi_{21} + \Pi_{23}. \tag{18}$$

In this instance equation (7) is rewritten as

$$\Pi_{\text{in}_2} = \Pi_{\text{diss}_2} + \Pi_{21} + \Pi_{23}, \tag{19}$$

which becomes, on substituting equation (18),

$$\Pi_{\text{in}_2} = \Pi_{\text{diss}_2} + \Pi_{\text{diss}_1} + \Pi_{\text{diss}_3}. \tag{20}$$

Thus in a similar manner to section 4.1, equation (20) may be rewritten:

$$(S_a/\omega^2) R_{\text{tot}} = (S_a/\omega^2) R_{\text{int}} + [V_1 S_{p_1}/(\rho c^2)]\beta_1 + [V_3 S_{p_3}/(\rho c^2)]\beta_3.$$

$$R_{\text{rad}} = \frac{\omega^2}{S_a \rho c^2}[S_{p_1} V_1 \beta_1 + S_{p_3} V_3 \beta_3], \tag{21}$$

$$R_{\text{rad}} = \frac{2\pi^2 c}{S_a \rho}[S_{p_1} n_1 \beta_1 + S_{p_3} n_3 \beta_3]. \tag{22}$$

It is seen that equation (22) reduces to equation (15) if one of the rooms (system 3) is eliminated. Equation (21) was used in the measurement of radiation resistance described in section 6.3.2.

4.3. COUPLING FACTOR FOR PANEL IN REVERBERANT ROOM

If a panel is suspended in a reverberant room and a loudspeaker is driven in the room, the power flow is given by equations (1) to (4) with $\Pi_{\text{in}_2} = 0$. Thus equation (3) becomes

$$0 = \Pi_{\text{diss}_2} - \Pi_{12}, \tag{23}$$

$$\eta_2 E_2 = \eta_{12} n_1 \left(\frac{E_1}{n_1} - \frac{E_2}{n_2}\right). \tag{24}$$

Now Lyon and Scharton [12] and Ungar and Scharton [14] have shown that under most conditions encountered in practice

$$\eta_{12} n_1 = \eta_{21} n_2. \tag{25}$$

But $\eta_{21} = \eta_{\text{rad}}^{4\pi}$ and $\eta_2 = \eta_{\text{int}}$, thus equation (24) may be rewritten:

$$\mu = \frac{\eta_{\text{rad}}^{4\pi}}{\eta_{\text{int}} + \eta_{\text{rad}}^{4\pi}} = \left(\frac{E_2}{n_2}\right) \Big/ \left(\frac{E_1}{n_1}\right), \tag{26}$$

which may be rewritten using the expressions given for E_1, E_2 and n_1 in section 4.1.:

$$\mu = [S_a/S_{p_1}]\Gamma^{-1}, \tag{27}$$

where

$$\Gamma = 2\pi^2 [n_p(\omega)/M_p](c/\rho). \tag{28}$$

Equations (27) and (28) give the result obtained by Lyon and Maidanik [3].

4.4. COUPLING FACTOR FOR PANEL BETWEEN ROOMS

If the panel is excited by driving a loudspeaker in each room, then the power flow is given by equations (5) to (10) with $\Pi_{\text{in}_2} = 0$. Thus equation (7) becomes

$$0 = \Pi_{\text{diss}_2} - \Pi_{12} - \Pi_{32}, \tag{29}$$

$$\eta_2 E_2 = \eta_{12} n_1 \left(\frac{E_1}{n_1} - \frac{E_2}{n_2}\right) + \eta_{32} n_3 \left(\frac{E_3}{n_3} - \frac{E_2}{n_2}\right). \tag{30}$$

Thus in a similar manner to section 4.3, equation (30) may be rewritten:

$$\mu = \frac{\eta_{\text{rad}}}{\eta_{\text{int}} + 2\eta_{\text{rad}}} = \frac{E_2}{n_2} \Big/ \left[\frac{E_1}{n_1} + \frac{E_3}{n_3}\right]; \tag{31}$$

$$\mu = [S_a/(S_{p_1} + S_{p_3})]\,\Gamma^{-1}, \tag{32}$$

where Γ is given by equation (28). Equation (32) reduces to equation (27) if one of the rooms is eliminated.

5. SOUND TRANSMISSION AND PANEL RESPONSE

It is assumed that the panel is clamped between the transmission room and the reception room of the transmission suite. Reverberant sound is produced in the transmission room by a loudspeaker. In this case the noise reduction, E_1/E_3, and consequently the sound transmission loss produced by the panel and also the panel vibration amplitude may be determined from equations (5) to (10) with $\Pi_{\text{in}_2} = 0$ and $\Pi_{\text{in}_3} = 0$.

5.1. PANEL TRANSMISSION LOSS

Putting $\Pi_{\text{in}_2} = 0$ in equation (8) and using equation (25), equation (33) is obtained:

$$\frac{E_2}{n_2} = \frac{\left(\frac{E_1}{n_1}\right)\eta_{21} - \left(\frac{E_3}{n_3}\right)\eta_{23}}{\eta_2 + \eta_{21} + \eta_{23}}; \tag{33}$$

but $\eta_{21} = \eta_{23} = \eta_{\text{rad}}$ and, except at low frequency where the present theory does not apply, $E_1/n_1 \gg E_3/n_3$, thus equation (33) becomes

$$\frac{E_2}{n_2} = \frac{E_1}{n_1}\left[\frac{\eta_{\text{rad}}}{\eta_{\text{int}} + 2\eta_{\text{rad}}}\right]. \tag{34}$$

Putting $\Pi_{\text{in}_3} = 0$ in equation (10) yields

$$E_3 = \frac{E_1\eta_{13} + E_2\eta_{23}}{\eta_3 + \eta_{31} + \eta_{32}}. \tag{35}$$

This is a similar result to that found by Lyon [13], except that no terms are neglected in the present analysis. The term $E_1\eta_{13}$ represents the mass law or non-resonant transmission since it occurs without the modes resonant in the frequency band under consideration being excited. The term $E_2\eta_{23}$ represents the resonant transmission.

Substituting equation (34) in equation (35) gives

$$\frac{E_3}{E_1} = \frac{\eta_{13} + \eta_{\text{rad}}^2(n_2/n_1)/(\eta_{\text{int}} + 2\eta_{\text{rad}})}{\eta_3 + (n_1/n_3)\eta_{13} + (n_2/n_3)\eta_{\text{rad}}}. \tag{36}$$

Equation (36) gives the noise reduction from the transmission to the reception room. The parameters η_{13}, η_{rad} and η_3 can be evaluated from the following equations:

$$\eta_{\text{rad}} = \frac{R_{\text{rad}}^{2\pi}}{\omega M_p}, \tag{37}$$

where the panel radiation resistance to half space $R_{\text{rad}}^{2\pi}$ is given by Maidanik [4] as

$$R_{\text{rad}}^{2\pi} = A_p\rho c.\begin{cases}(\lambda_c\lambda_a/A_p)\,2(f/f_c)\,g_1(f/f_c) + (P\lambda_c/A_p)\,g_2(f/f_c), & f<f_c;\\ (l_1/\lambda_c)^{-1/2} + (l_2/\lambda_c)^{1/2}, & f=f_c;\\ (1-f_c/f)^{-1/2}, & f>f_c,\end{cases} \tag{38}$$

where

$$g_1(f/f_c) = \begin{cases} (4/\pi^4)(1-2\alpha^2)/\alpha(1-\alpha^2)^{1/2}, & f < \tfrac{1}{2} f_c, \\ 0, & f > \tfrac{1}{2} f_c, \end{cases}$$

$$g_2(f/f_c) = (2\pi)^{-2}\{(1-\alpha^2)\ln[(1+\alpha)/(1-\alpha)] + 2\alpha\}/(1-\alpha^2)^{3/2},$$

$$\alpha = (f/f_c)^{1/2}.$$

It should be noted that the expression for $f < f_c$ given in reference 4 was in error, but the correct expression [21] (communicated by Maidanik), is given in equation (38). The expression for $f > f_c$ given in reference 4 was also incorrect and this has been corrected above.

The coupling loss factor η_{13} due to non-resonant mass-law transmission is obtained from [13]:

$$10\log_{10}\eta_{13} = -\text{T.L.} + 10\log_{10}\left(\frac{A_p c}{4V_1\omega}\right), \tag{39}$$

where T.L. is the random incidence mass law transmission loss value for the second system (the panel). Finally,

$$\eta_3 = \frac{2\cdot 2}{f T_3}. \tag{40}$$

If equations (37), (38), (39) and (40) are evaluated and a value for η_{int} is chosen, or else measured by experiment, then the noise reduction N.R. (in dB) can be evaluated by taking logs of equation (36):

$$\begin{aligned} \text{N.R.} = {} & 10\log_{10}[\eta_{13} + \eta_{\text{rad}}^2(n_2/n_1)/(\eta_{\text{int}} + 2\eta_{\text{rad}})] - \\ & -10\log_{10}[\eta_3 + (n_1/n_3)\eta_{13} + (n_2/n_3)\eta_{\text{rad}}], \end{aligned} \tag{41}$$

where the room modal densities are

$$\left.\begin{aligned} n_1 &= \frac{V_1\omega^2}{2\pi^2 c^3}, \\ n_3 &= \frac{V_3\omega^2}{2\pi^2 c^3}. \end{aligned}\right\} \tag{42}$$

The transmission loss is then

$$\text{T.L.} = \text{N.R.} + 10\log_{10}\left[\frac{A_p c T_3}{24 V_3 \ln(10)}\right]. \tag{43}$$

5.2. RESPONSE OF PANEL

The panel vibration amplitude is given by equation (34). For a reverberant field the total energy in a 1 Hz bandwidth $E_1 = S_{p_1} V_1/(\rho c^2)$, and the total panel energy in a 1 Hz bandwidth $E_2 = M_p S_a/\omega^2$; hence equation (34) becomes

$$\frac{M_p S_a}{n_2 \omega^2} = \frac{S_{p_1}}{\rho c^2}\frac{V_1}{n_1}\frac{\eta_{\text{rad}}}{\eta_{\text{int}} + 2\eta_{\text{rad}}}. \tag{44}$$

The modal density of the transmission room $n_1(\omega) = V_1\omega^2/(2\pi^2 c^3)$, while the modal density of the panel $n_2(\omega) = \sqrt{3}A_p/(2\pi h c_l)$, and the critical frequency $f_c = \sqrt{3}c^2/(\pi h c_l)$, thus

$$\frac{S_a}{S_{p_1}} = \frac{\eta_{\text{rad}}}{\eta_{\text{int}} + 2\eta_{\text{rad}}}\frac{\pi^2 f_c}{\rho_s \rho c}. \tag{45}$$

If the panel responded as a limp mass, the response would be

$$\frac{S_{a_{\text{m.l.}}}}{S_{p_w}} = \frac{1}{\rho_s^2}, \tag{46}$$

where S_{p_w} is the pressure spectral density at the panel surface. Neglecting panel motion, $S_{p_w} = 2S_{p_1}$, since there is pressure doubling for each wave arriving at the panel surface, although at any instant only half the waves are travelling towards the panel. Thus,

$$\frac{S_{a_{m.l.}}}{S_{p_1}} = \frac{2}{\rho_s^2}. \tag{47}$$

Dividing equation (45) by equation (47) gives the panel response relative to mass law:

$$\frac{S_a}{S_{a_{m.l.}}} = \frac{\eta_{rad}}{\eta_{int} + 2\eta_{rad}} \frac{\pi^2 f_c \rho_s}{2\rho c}. \tag{48}$$

6. EXPERIMENTAL MEASUREMENTS

Experiments were made to measure the radiation resistance, the total resistance, the coupling factor, the modal density, the transmission loss and the vibration response of an aluminium panel. The panel was $\frac{1}{8}$ in. thick and measured 77·5 by 61·0 in. when clamped in a frame. In some of the following experiments the panel was suspended from two corners in an anechoic room or in a 4500 ft^3 reverberant room. In these experiments the panel was surrounded by a 2 ft wide baffle and the narrow gap between the panel and baffle was sealed

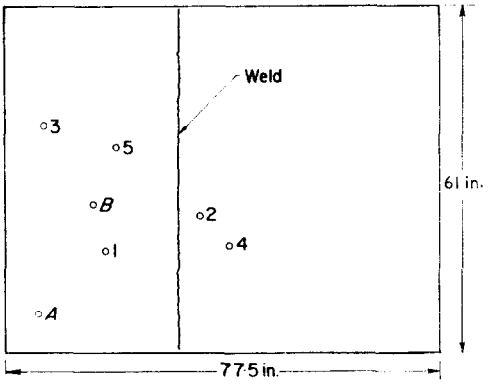

Figure 5. Positions on panel.

with a plastic tape. In the other experiments described here the panel was clamped in a frame between the transmission and reception rooms. The panel edge conditions were intended to be fully fixed and the frame was attached to the reception room (Figure 3) which was vibration-isolated from the transmission room with glass fibre. Unless otherwise stated the experiments in section 6 were conducted by supplying $\frac{1}{3}$-octave bands of white noise to the loudspeakers or shakers in use. Panel measurement positions are shown in Figure 5.

6.1. MEASUREMENTS OF PANEL MODAL DENSITY

The panel was suspended in an anechoic room and excited by a loudspeaker producing acoustic waves at grazing incidence and in a direction diagonally across the panel. The experimental arrangement is shown in Figure 6, where the sine-wave generator was driven at a very low speed from the level recorder. The output from an accelerometer was fed into the level recorder. A typical result is shown in Figure 7. The modal density was computed by counting the number of modes in a given frequency band and dividing by the bandwidth.

For a simply-supported panel the modal density is

$$n_p(f) = \frac{\sqrt{3} A_p}{c_l h}. \tag{49}$$

For aluminium, the speed of longitudinal waves is $c_l \approx 17{,}000$ ft/sec, and for the panel, $A_p = 37{\cdot}6\ \text{ft}^2$, $h = 1/96$ ft. Hence the modal density is

$$n_p(f) = 0{\cdot}36 \text{ modes/Hz}.$$

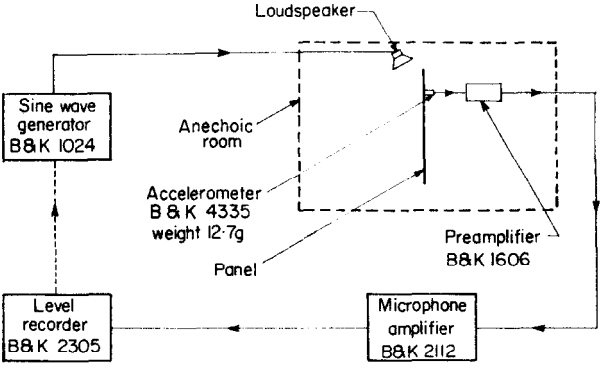

Figure 6. Experimental apparatus to measure panel modal density.

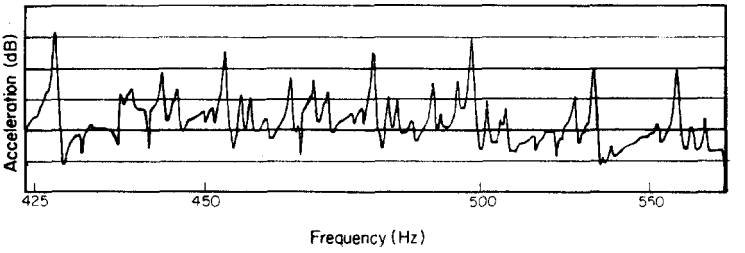

Figure 7. Modal resonances in panel.

Figure 8 shows that except at very low frequency (<20 Hz) the agreement between theory and experiment is good. The experiment was repeated with the panel clamped between the rooms.

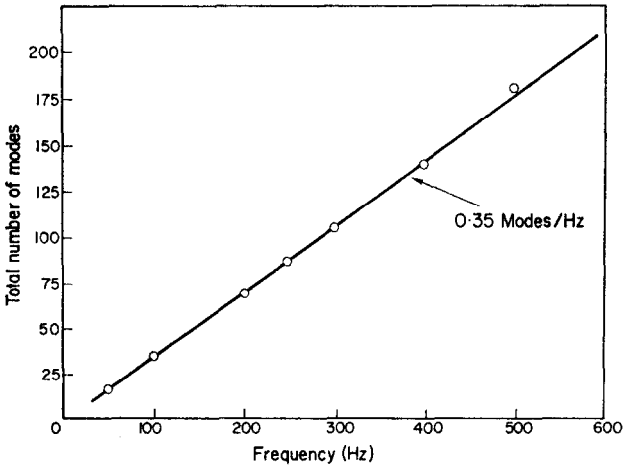

Figure 8. Modal density of panel.

The clamping reduced the area to 32·9 ft^2 and hence the theoretical modal density to 0·315 modes/Hz. This compared with a measured value of 0·303 in the mid-frequency range (about 500 Hz).

6.2. MEASUREMENT OF TOTAL RESISTANCE

The apparatus used is shown schematically in Figure 9. The panel was clamped at its edges between the two rooms and excited with a shaker near to one corner (Figure 5, position A). The panel damping was determined from decay measurements when excitation was abruptly terminated. Use of discrete tone excitation instead of $\frac{1}{3}$-octave bands of white noise ap-

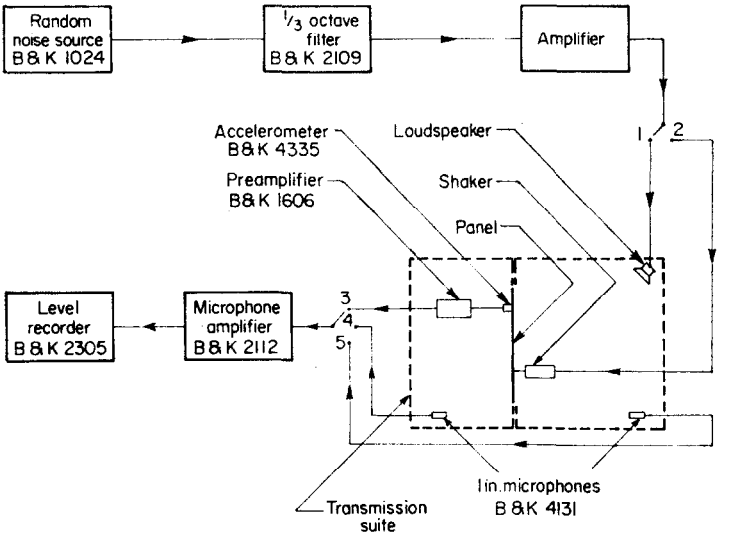

TABLE

Measurement	Switch positions
Total resistance	2, 3
Radiation resistance	2, 4 and 5
Noise transmission	1, 4 and 5
Vibration response	1, 3

Figure 9. Apparatus used to measure panel total resistance, radiation resistance, noise transmission and vibration response.

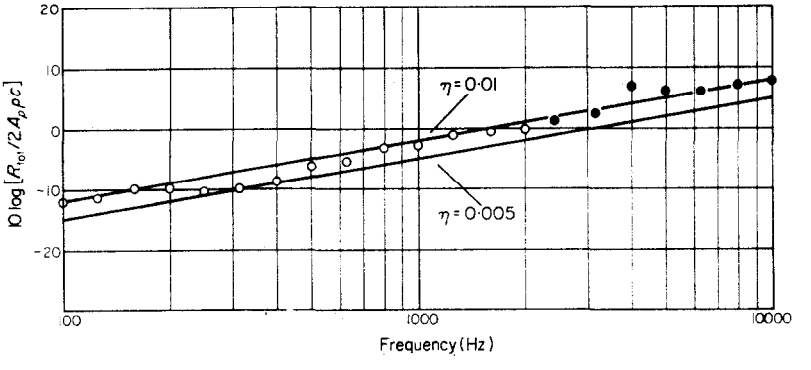

Figure 10. Normalized total resistance of panel: direct measurement (○); measured using reduced playback speed on tape-recorder (●).

peared to give rather inconsistent results, depending upon whether or not the frequency coincided with a modal resonance [22]. Due to limitations in the writing speed of the level

corder it was only possible to measure directly the total resistance of the panel up to 2000 Hz. Above this frequency it was necessary to use a tape-recorder and play back the signal at a slower speed. The plot of normalized total radiation resistance is given in Figure 10. The total resistance† was determined from

$$R_{tot} = (13{\cdot}8/T_2)\, M_p.$$

6.3. MEASUREMENT OF RADIATION RESISTANCE

6.3.1. *Baffled panel in reverberant room*

The panel was excited by a shaker attached at position B. The pressure levels were measured at two points in the room and the acceleration was measured at positions 2 and 3 on the panel

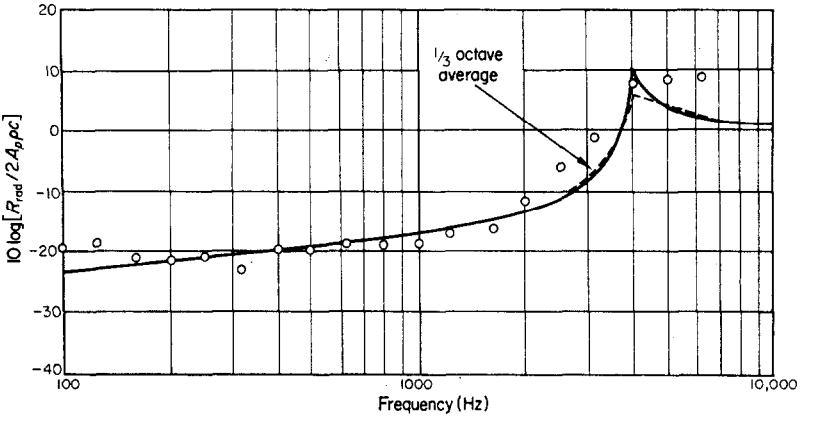

Figure 11. Normalized radiation resistance—baffled panel.

(see Figure 5). The reverberation time of the room against frequency was measured. The radiation resistance was calculated using equation (14) and averaged values of S_{p_1} and S_a. The results are plotted in Figure 11.

6.3.2. *Panel between rooms*

The radiation resistance was measured in a similar manner to section 6.3.1. The panel was excited by a shaker attached at position *A*. The pressure levels were measured at five positions

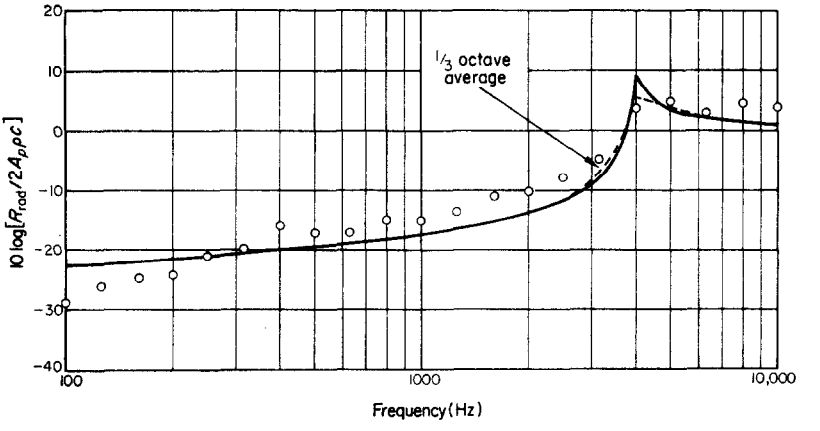

Figure 12. Normalized radiation resistance—panel between two rooms.

† It should be noted that the total resistance $R_{tot} = \beta M_p = \eta\omega M_p = 2\delta\omega M_p$.

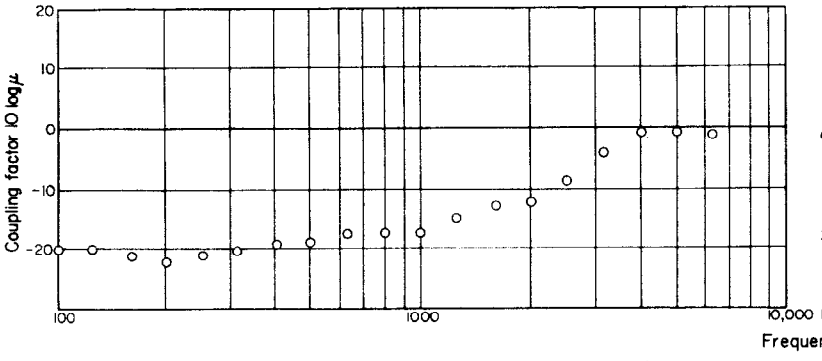

Figure 13. Coupling factor for baffled panel.

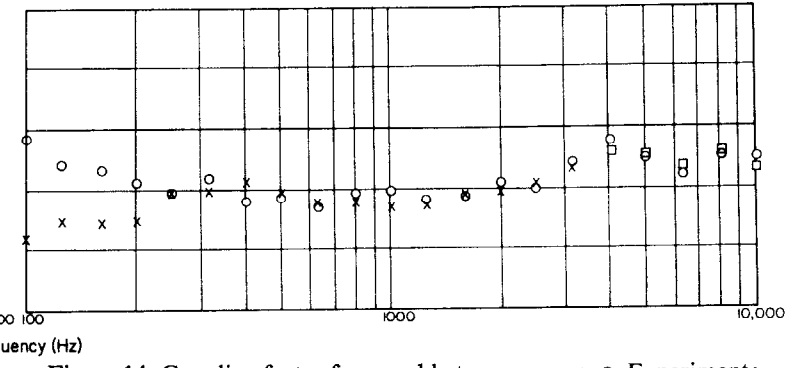

Figure 14. Coupling factor for panel between rooms. ○, Experiment; ×, deduced from measured $R_{\text{rad}}^{2\pi}$ and R_{tot}; □, deduced from measured $R_{\text{rad}}^{2\pi}$ and $\eta_{\text{int}} = 0{\cdot}01$.

in each room and the acceleration at five points on the panel (see Figure 5). The reverberation times of each room were measured (as a function of frequency) and the radiation resistance was calculated from equation (21) using averaged values of S_{p_1}, S_{p_3} and S_a. The result is plotted in Figure 12.

6.4. MEASUREMENT OF PANEL COUPLING FACTOR

6.4.1. *Baffled panel in reverberant room*

The panel was excited with reverberant white noise in $\frac{1}{3}$-octave bands from a loudspeaker at one corner in the room. The acceleration level was measured at five points on the panel and the pressure level at five points in the room. The coupling factor was calculated using equations (27) and (28) and arithmetically averaged values of S_{p_1} and S_a. The result is plotted in Figure 13.

6.4.2. *Panel between rooms*

The panel was again excited with reverberant white noise in $\frac{1}{3}$-octave bands. The noise was produced by feeding the same signal through different amplifiers to a loudspeaker in each room. At the beginning of the experiment the amplifier gains were adjusted until the levels in each room were approximately the same throughout the frequency range. The gains were then kept constant throughout the experiment. The acceleration level was measured at five points on the panel and the pressure level at five points in the room. The coupling factor was calculated using equations (32) and (28). The result is shown in Figure 14.

6.5. MEASUREMENT OF TRANSMISSION LOSS AND PANEL RESPONSE

6.5.1. *Transmission loss*

The panel was placed between the two large reverberant rooms (Figure 3). $\frac{1}{3}$-octave bands of white noise were made in the transmission room with a loudspeaker (Figure 9) and the levels recorded in each room. This was repeated at five positions of the microphone in each room. The reverberation time of the reception room was measured as a function of frequency. A plot of transmission loss calculated by the theory of section 5.1 is given in Figure 15.

6.5.2. *Panel response*

At the same time as the transmission loss experiment described above was performed, the acceleration of the panel was measured for five different panel positions (Figure 5). The panel response compared with mass law was calculated from equation (48) and is plotted in Figure 17.

7. DISCUSSION OF EXPERIMENTAL RESULTS

The total resistance of a panel R_{tot} is the sum of the internal resistance R_{int} and the radiation resistance R_{rad}. At low frequency, where the radiation resistance is small, the resistance of the panel is mostly due to the internal resistance. At the critical frequency the resistance is mostly due to the radiation resistance, but well above coincidence the total resistance again normally becomes dominated by the internal resistance. The measured values of total resistance, in general, tended to confirm the above hypotheses. Figure 10 shows that the total resistance lies between $\eta_{\text{tot}} = 0{\cdot}005$ and $0{\cdot}01$, below coincidence. This value agrees fairly closely with the value measured by Lyon for a similar sized aluminium panel of $\frac{1}{16}$ in. thickness [12].

The measurements of radiation resistance appear to agree well with the theory (Figures 11 and 12). The panel in Figure 11 was freely supported and baffled, while the panel in Figure 12 had clamped edges. The panel assumed in the theoretical comparison had simply-supported

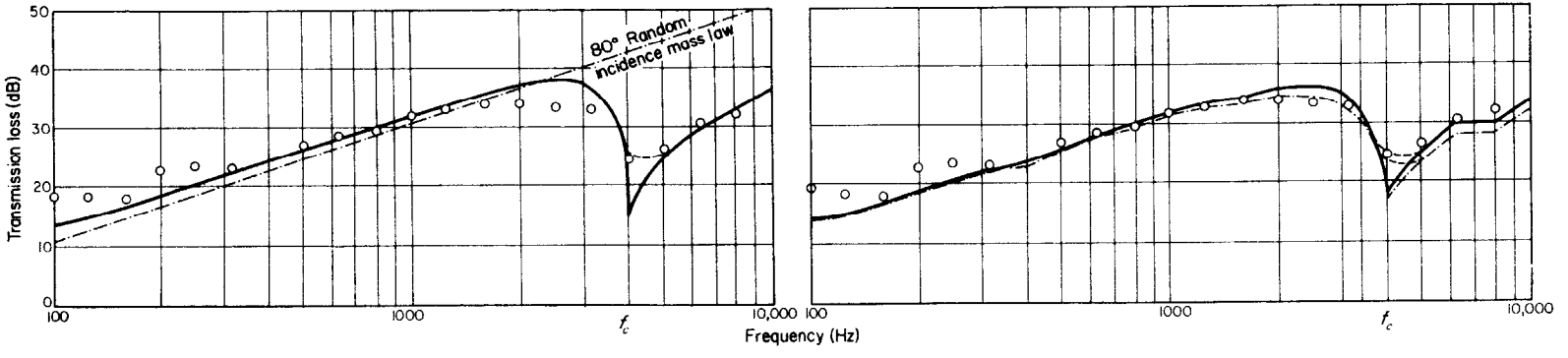

Figure 15. Experimental values of panel transmission loss compared with theoretical prediction. ---, $\frac{1}{3}$-octave average; ——, $\eta_{int} = 0{\cdot}005$.

Figure 16. Comparison of experimental panel transmission loss with prediction using experimental values of R_{rad} for two values of η_{int}. ---, $\frac{1}{3}$-octave average; ——, $\eta_{int} = 0{\cdot}01$; —·—, $\eta_{int} = 0{\cdot}005$.

edges and the weld was assumed to act as a rib. It is probable that the difference in the mid-frequency range between Figures 11 and 12 is due to the different edge conditions. Maidanik states [4] that at low frequencies the radiation resistance of a clamped panel should be twice that of a simply-supported panel. The difference between the theoretical and experimental results in Figure 11 may be due to the inefficiency of the baffle at low frequencies.

The coupling of the panel with the rooms is shown in Figures 13 and 14. In the first case the coupling factor $\mu = R_{rad}/[R_{int} + R_{rad}]$. As expected the coupling factor $\mu \to 1$ above coincidence because $R_{rad} \gg R_{int}$ at and just above coincidence when the panel was freely-supported. However, when the panel was clamped between the two rooms, the coupling factor became $\mu = \frac{1}{2}R_{rad}/[R_{int} + R_{rad}]$ and the internal resistance was increased considerably. Thus, as expected, at and just above coincidence $\mu \to 0{\cdot}5$; also as the frequency increases above

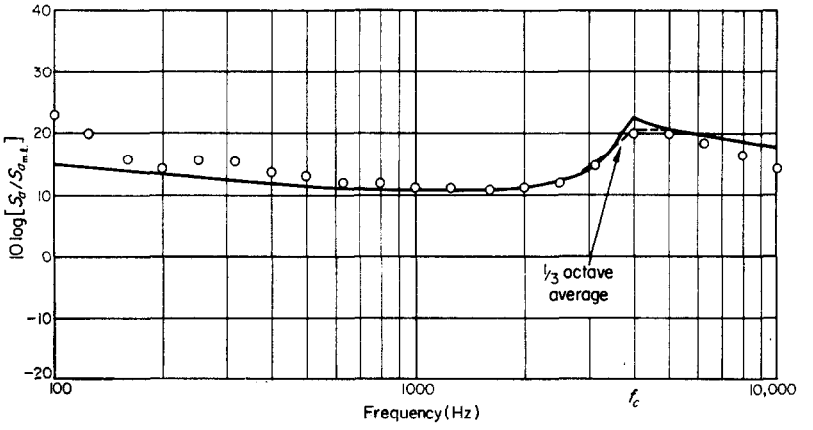

Figure 17. Panel response relative to mass law. $\eta_{int} = 0{\cdot}005$.

coincidence μ decreases again, due to the rapid relative increase in R_{int}. The agreement between the values of μ given in Figure 14 found from experiment (section 6.4.2) and those determined from experimental values of R_{rad} and R_{tot} is satisfactory, except at low frequency (<400 Hz). It is thought that the low-frequency disagreement, which is considerable, is due to the low-frequency panel/room modal interaction. At low-frequencies there are insufficient panel modes to make a correct average, a fact which is not included in the present theory.

Figure 15 shows a comparison between the transmission loss of the panel measured experimentally and that calculated using the theory of section 5.1. The value of η_{int} used in the theoretical calculation was 0·005 and the theoretical values of η_{rad} used were determined from Maidanik's expressions for a simply-supported panel [equation (38)]. It is seen that agreement between experiment and theory is good, with two exceptions. These are at low frequency (<400 Hz) and just below coincidence. The low-frequency disagreement is again thought to be due to room mode/panel mode coupling as also observed in the coupling factor experiment and discussed above. The apparent discrepancy just below coincidence is removed if experimental values of η_{rad} are used in the calculations (see Figure 16).

The measured acceleration level of the panel above mass law as compared with that predicted by the theory is given in Figure 17. For the theoretical prediction a value of $\eta_{int} = 0{\cdot}005$, and η_{rad} determined from Maidanik's expressions were again used. A similar low-frequency discrepancy to that observed in the other experiments was again apparent. The agreement is otherwise remarkably good. Above coincidence the experimental values start to fall below the theoretical curve; part of this disagreement above coincidence is probably

due to mass loading of the panel by the accelerometer. No correction was made for mass loading which was expected to be of the order of 1 or 2 dB in this frequency region.

8. CONCLUSIONS

"Statistical energy analysis" has been shown to provide a useful way of predicting the transmission loss of a panel. This analysis obviously has its uses in classical architectural transmission loss problems as well as in aerospace transmission loss predictions. The vibration amplitude of a partition has also been satisfactorily predicted thus explaining the previously observed discrepancy [1] between the experimental partition response and that predicted by mass law.

ACKNOWLEDGMENTS

The authors would like to thank Dr R. H. Lyon and Dr G. Maidanik for discussions and helpful comments and suggestions. The authors are indebted to Professor H. D. Parbrook for his encouragement. The research was supported by the Science Research Council.

REFERENCES AND BIBLIOGRAPHY

1. W. A. Utley and K. A. Mulholland 1967 *J. Sound Vib.* **6**, 419. Measurement of transmission loss using vibration transducers.
2. P. W. Smith 1962 *J. acoust. Soc. Am.* **34**, 640. Response and radiation of structural modes excited by sound.
3. R. H. Lyon and G. Maidanik 1962 *J. acoust. Soc. Am.* **34**, 623. Power flow between linearly coupled oscillators.
4. G. Maidanik 1962 *J. acoust. Soc. Am.* **34**, 809. Response of ribbed panels to reverberant acoustic fields.
5. R. H. Lyon 1962 *J. acoust. Soc. Am.* **35**, 1265. Sound radiation from a beam attached to a plate.
6. P. W. Smith and R. H. Lyon 1965 *NASA CR*-160. Sound and structural vibration.
7. E. Buckingham 1925 *Scientific Papers of the Bureau of Standards No.* 506. Theory and interpretation of experiments on the transmission of sound through partition walls.
8. A. L. Kimball 1936 *J. acoust. Soc. Am.* **7**, 222. Theory of transmission of plane sound waves through multiple partitions.
9. L. L. Beranek and G. A. Work 1949 *J. acoust. Soc. Am.* **21**, 419. Sound transmission through multiple structures containing flexible blankets.
10. A. London 1949 *J. Research Nat. Bur. of Stand.* **42**, RP 1998, 605. Transmission of reverberant sound through single walls.
11. A. London 1950 *J. acoust. Soc. Am.* **22**, 270. Transmission of reverberant sound through double walls.
12. R. H. Lyon and T. D. Scharton 1965 *J. acoust. Soc. Am.* **38**, 253. Vibrational-energy transmission in a three-element structure.
13. R. H. Lyon 1966–67 Lecture notes from *Bolt, Beranek and Newman Inc. Program for Advanced Study—Aerospace Noise and Vibration, Los Angeles.* Ch. IX.
14. E. E. Ungar and T. D. Scharton 1967 *Shock Vibr. Bull.* **36**, Pt. 5, 41. Analysis of vibration distributions in complex structures.
15. R. H. Lyon, C. W. Dietrich, E. E. Ungar, R. W. Pyle and R. E. Apfel 1966 *NASA CR*-589. Low-frequency noise reduction of spacecraft structures.
16. R. H. Lyon and E. Eichler 1964 *J. acoust. Soc. Am.* **36**, 1344. Random vibration of connected structures.
17. E. Eichler 1965 *J. acoust. Soc. Am.* **37**, 995. Thermal circuit approach to vibrations in coupled systems and the noise reduction of a rectangular box.
18. D. E. Newland 1968 *J. acoust. Soc. Am.* **43**, 553. Power flow between a class of coupled oscillators.
19. E. E. Ungar 1966 *AFFDL-TR*-66-52. Fundamentals of statistical energy analysis of vibrating systems.
20. R. H. Lyon 1967 *Shock and Vibration Information Center, United States Department of Defence, Monograph SVM*-1. Random noise and vibration in space vehicles.
21. G. Maidanik 1968 Private Communication.
22. A. J. Price and M. J. Crocker 1968 *University of Liverpool, Department of Building Science Report BS/A/68*-2. The theory and measurement of radiation from panels.

APPENDIX: LIST OF SYMBOLS

A_p panel surface area
c speed of sound in air
c_l speed of longitudinal panel waves
E_i total energy in ith system
f frequency
f_c critical or coincidence frequency
g_1, g_2 functions of f/f_c
h panel thickness
i, j integer subscripts representing system numbers ($i = 1, 2, 3$ and $j = 1, 2, 3$)
l_1, l_2 length, breadth of panel
M_p total panel mass modal density of ith system in radian frequency
n_i model density of the ith system in radian frequency
n_p modal density of panel
P perimeter of panel (including twice length of weld)
R_{int} internal resistance of panel
R_{rad} radiation resistance of panel to whole space
$R_{\text{rad}}^{2\pi}$ radiation resistance of panel to half space
R_{tot} total resistance of panel
S_a spectral density of panel acceleration
$S_{a_{\text{m.l.}}}$ spectral density of panel acceleration predicted by mass law
S_{p_1} spectral density of pressure in transmission room or reverberant room
S_{p_2} spectral density of pressure in reception room
S_v spectral density of panel velocity
T_i reverberation time of ith system
V_1 volume of transmission room or reverberant room
V_3 volume of reception room
β_1 energy decay constant for transmission room or reverberant room
β_3 energy decay constant for reception room
η_i internal loss factor for ith system
η_{ij} coupling loss factor from ith to jth system
η_{int} internal loss factor for panel
η_{rad} radiation loss factor for panel (to half space)
$\eta_{\text{rad}}^{4\pi}$ radiation loss factor for panel (to whole space)
η_{tot} total loss factor for panel
λ_a acoustic wavelength
λ_c coincidence wavelength of panel
μ coupling factor between acoustic field and panel
Π_{ij} power flow from ith to jth system
Π_{diss_i} power dissipated internally by ith system
Π_{in_i} power supplied to ith system
ρ air density
ρ_s panel surface density
ω angular frequency